3D MHD Models of Active Region Loops

Leon Ofman

Department of Physics, Catholic University of America, and NASA Goddard Space Flight Center, Code 682, Greenbelt, MD 20771, USA

Abstract

Present imaging and spectroscopic observations of active region loops allow to determine many physical parameters of the coronal loops, such as the density, temperature, velocity of flows in loops, and the magnetic field. However, due to projection effects many of these parameters remain ambiguous. Three dimensional imaging in EUV by the STEREO spacecraft will help to resolve the projection ambiguities, and the observations could be used to setup 3D MHD models of active region loops to study the dynamics and stability of active regions. Here the results of 3D MHD models of active region loops are presented, and the progress towards more realistic 3D MHD models of active regions. In particular the effects of impulsive events on the excitation of active region loop oscillations, and the generation, propagations and reflection of EIT waves are shown. It is shown how 3D MHD models together with 3D EUV observations can be used as a diagnostic tool for active region loop physical parameters, and to advance the science of the sources of solar coronal activity.

Key words: Solar Corona, STEREO Spacecraft, Coronal Loops, Coronal Active Regions, MHD, Waves, Numerical Simulation Studies

1 Introduction

The Solar TErrestrial RElations Observatory (STEREO) is currently in its development phase, and is scheduled to launch in 2006. The two STEREO spacecraft (see figure 1) will provide stereoscopic imaging which will allow to reconstruct coronal structures in 3D. Extreme Ultraviolet Imager (EUVI) will provide full Sun coverage with twice the spatial resolution and dramatically improved cadence over SOHO/EIT.

There is ample observational evidence for wave activity in coronal active region loops in EUV by TRACE, SOHO/EIT, and SUMER (e.g., Aschwanden, et al., 1999; Nakariakov et al., 1999; Nakariakov & Ofman, 2001; Aschwanden, et al, 2002; Schrijver, et al., 2002; Kliem, et al., 2002; De Moortel, et

al., 2000, 2002; Wang et al., 2002; Ofman & Wang, 2002; Wang et al., 2003), and of global EIT waves (e.g., Thompson et al., 1999; Wills-Davey & Thompson, 1999; Biesecker et al., 2002). The waves are low-frequency with periods on the order of minutes and long wavelength (order of 10^5 km), and can be modelled well by MHD equations. Motivated by the observations theoretical models have been developed for coronal loop oscillations (Nakariakov et al., 1999; Roberts, 2000; Nakariakov & Ofman, 2001; Ruderman & Roberts, 2002; Ofman & Aschwanden, 2002; Ofman & Wang, 2002; Goossens, et al., 2002; Ruderman, 2003; Mendoza-Briceño, et al., 2004; Terradas & Ofman, 2004a), and for global EIT waves (Wu, et al., 2001; Ofman & Thompson, 2002; Terradas & Ofman, 2004b).

In figure 2 an example of oscillations observed in a coronal loop arcade by TRACE at 171 Å on April 15, 2001 is shown. The event was analyzed by Aschwanden, et al (2002), and Verwichte et al. (2004), and the basic parameters such as frequency and damping time of the oscillations were determined. However, due to the lack of 3D information the length of the individual loops and the interaction between them due to their spatial orientation is poorly known. These parameters are needed to determine the wave mode, and to compare to wave theories and MHD models, which than can be used to determine the properties of the active region plasma, and the magnetic field strength. The STEREO mission will be able to provide this information for similar events, and the physical parameters of the oscillations could be established.

In figure 3 Doppler velocity oscillations observed by SUMER on April 15, 2002 are shown. The identification of the loop and the geometry of the structure was modelled using EIT 195 Å. The determination of the 3D loop geometry is important for the correct identification of the MHD wave mode, and the wavelength. However, the 3D information is not currently available. With the launch of the STEREO mission 3D structure of similar loops will be observed, thus improving the analysis of such loop oscillations.

The STEREO observations will provide the information that could be used to initiate 3D MHD models of loops and active regions. The MHD models of waves in an active regions can be used as a diagnostic tool for the physical properties of the active regions, such as magnetic field and density structure. First studies of 3D MHD models of waves in active regions were performed by Ofman & Thompson (2002), and Terradas & Ofman (2004a,b). However, theoretical difficulties remain due to the complexity of the damped MHD wave modes in nonhomogeneous media, nonlinearity, boundary conditions, and observational uncertainties.

2 Dissipative 3D MHD Model and Boundary Conditions

The resistive 3D MHD equations in *cgs* units with the usual notations for the variables are

$$\frac{\partial \rho}{\partial t} + \nabla \cdot (\rho \mathbf{V}) = 0, \tag{1}$$

$$\rho \left[\frac{\partial \mathbf{V}}{\partial t} + (\mathbf{V} \cdot \nabla)\mathbf{V} \right] = -\nabla p - \frac{GM_{\odot}\rho}{r^2} + \frac{1}{c}\mathbf{J} \times \mathbf{B}, \tag{2}$$

$$\frac{\partial \mathbf{B}}{\partial t} = -c\nabla \times \mathbf{E}, \text{ where } \mathbf{E} = -\frac{1}{c}\mathbf{V} \times \mathbf{B} + \eta \mathbf{J}, \tag{3}$$

$$\nabla \times \mathbf{B} = \frac{4\pi}{c}\mathbf{J}, \tag{4}$$

$$\frac{\partial T}{\partial t} = -(\gamma - 1)T\nabla \cdot \mathbf{V} - \mathbf{V} \cdot \nabla T + (\gamma - 1)(H_{in} - H_{loss}). \tag{5}$$

In the above equations viscosity was neglected, and the isothermal approximation was used ($\gamma = 1$) for the studies presented here. Thus the heat input due to coronal heating H_{in} and heat losses H_{loss} due to conduction, and radiation were not modelled explicitly. The resistive 3D MHD equations in Cartesian geometry were solved numerically in a box defined by $x_{min} < x < x_{max}$, $y_{min} < y < y_{max}$, $z_{min} < z < z_{max}$ using the modified Lax-Wendroff method with fourth order artificial viscosity added for stability.

2.1 Boundary and Initial Conditions

For the 3D MHD models of loop oscillations the loops were initialized with a single, or four cylindrical flux tubes with an Alfvén speed decrease by about a factor of three inside the loop compared to the Alfvén speed outside the loop. The boundary conditions applied at the 6 planes defined by x_{min}, x_{max}, y_{min}, y_{max}, z_{min}, z_{max} were as follows: line tied boundary conditions at both ends of the loops that allow flows parallel to the loop axis through the ends of the loops (these flows were found to be small in the model). The boundary conditions were open (i.e., extrapolated variables) in the planes parallel to the loop axis. These boundary conditions can be written as

$$\begin{aligned}
&\mathbf{B}(x, y, z_{min,max}, t) = \mathbf{B}(x, y, z_{min,max} \pm \Delta z, t), \\
&V_x(x, y, z_{min,max}, t) = 0, \\
&V_y(x, y, z_{min,max}, t) = 0, \\
&V_z(x, y, z_{min,max}, t) = V_z(x, y, z_{min,max} \pm \Delta z, t), \\
&\rho(x, y, z_{min,max}, t) = \rho(x, y, z_{min,max} \pm \Delta z, t),
\end{aligned} \tag{6}$$

where Δz is the grid separation in the z-direction, the positive sign corresponds to z_{min}, and the negative sign to z_{max}. Open boundary conditions were used at the other 4 boundary planes. At x_{min}, and at x_{max} the boundary conditions were

$$\begin{aligned}
&\mathbf{B}(x_{min,max}, y, z) = \mathbf{B}(x_{min,max} \pm \Delta x, y, z), \\
&\mathbf{V}(x_{min,max}, y, z) = \mathbf{V}(x_{min,max} \pm \Delta x, y, z), \\
&\rho(x_{min,max}, y, z) = \rho(x_{min,max} \pm \Delta x, y, z),
\end{aligned} \tag{7}$$

where Δx is the grid separation in the x-direction, the positive sign corresponds to x_{min}, and the negative sign corresponds to x_{max}. Similar expressions were used for the boundary conditions at $y_{min,max}$. For the initial perturbation a fast magnetosonic wave was launched from the boundary of the computational domain towards the loop (see, figure 4).

For the 3D MHD model of the active region line-tied boundary conditions that do not allow flow through the boundary were applied at the lower boundary, and open boundary conditions on the remaining five planes as follows:

$$\begin{aligned}
&\mathbf{B}(x, y, z_{min}, t) = \mathbf{B}_0(x, y, z_{min}), \\
&\mathbf{V}(x, y, z_{min}, t) = 0, \\
&\rho(x, y, z_{min}, t) = \rho(x, y, z_{min}, t = 0).
\end{aligned} \tag{8}$$

Open boundary conditions were applied at the other 5 boundary planes. At x_{min}, and at x_{max} the boundary conditions were

$$\begin{aligned}
&\mathbf{B}(x_{min,max}, y, z) = \mathbf{B}(x_{min,max} \pm \Delta x, y, z), \\
&\mathbf{V}(x_{min,max}, y, z) = \mathbf{V}(x_{min,max} \pm \Delta x, y, z), \\
&\rho(x_{min,max}, y, z) = \rho(x_{min,max} \pm \Delta x, y, z),
\end{aligned} \tag{9}$$

where the positive sign corresponds to x_{min}, and the negative sign corresponds to x_{max}. Similar expressions were used for the boundary conditions at $y_{min,max}$, and at z_{max}.

To model the impact of an EIT wave an initial velocity pulse was imposed at $y = y_{min}$

$$V_y(x, y_{min}, z, t) = V_0, \quad 0 < t < \delta t, \tag{10}$$

where the duration of the pulse is $\delta t = 10\ \tau_A$, where τ_A is the Alfvén time, $V_0 = 0.04$ is the initial amplitude of the pulse. After a transit time of $5\tau_A$ following the pulse, the boundary condition on V_y at $y = y_{min}$ becomes open.

The line-of-sight component of the photospheric magnetic field taken from Kitt-Peak magnetogram smoothed down to MHD model resolution (see, figure 7a) was used for potential extrapolation, and the resulting field was used as the initial condition, as well as the lower boundary magnetic field. Gravity, and the gravitationally stratified density with $n = 10^{10}$ at the lower boundary and $T = 2 \times 10^6$ K throughout the active region were used in the model. Thus, the resulting active region model was non potential. However, due to the small plasma β (ratio of thermal to magnetic pressure) the nonpotential effects were small. The Lundquist number was 10^3, appropriate for the resolution used in the model ($133 \times 71 \times 102$). Initially, the time-dependent 3D MHD model was evolved to a quasi-steady state following the launch of the fast magnetosonic wave at the boundary of the computational domain (see, figure 7b).

3 Numerical Results

In this section the results of 3D MHD modelling of active region loop oscillations are shown. The typical temporal evolution of a loop velocity due to the impact of a fast magnetosonic wave is shown in figure 5 at a location near the midpoint of the loop length, and near the loop boundary ($x = 1.07$, $y = 2.70$, $z = 8.04$ in normalized units). In this case the loop length was $L = 15.7$, the loop radius was $a = 1$, and the size of the simulation box was $15.7 \times 5.4 \times 5.4$ units, and the resolution was $110 \times 110 \times 130$. The Lundquist number S for this loop was 10^3, and was increased to 10^4 in high resolution runs ($230 \times 230 \times 130$). Initially, the velocity variations exhibit strong fluctuations following the impact of the waves. However, the higher harmonic fluctuations, damp quickly, and the long wavelength mode becomes dominant and damps at a slower rate. In the top panel of figure 5 the V_x component of the velocity that corresponds to the transverse oscillations of the loop near the center is shown. The lower panel shows the V_y component, that correspond to the torsional Alfvén waves excited in the loop (e.g, Ofman & Davila, 1995). The magnitude of the V_y component peaks near the loop boundary due to the resonant absorption, and is small outside that boundary layer of the loop. The V_y reverses sign in the resonant absorption layer and is associated with the torsional Alfvén wave (see, for example Ofman, et al., 1994; Ofman & Davila, 1995, for more details).

Figure 6 shows the scaling with the Lundquist number S of the damping time of the loop oscillations for a single loop and for a bundle of four loops that represent multithreaded loop. It is evident that for a single loop the damping time is nearly independent of the Lundquist number. However, for the multithreaded loop the damping time increases with the Lundquist number. The increase is initially close to the phase mixing scaling of $S^{1/3}$ (show with the dashed line). However, at large Lundquist numbers the damping time does not

increase as fast with S, due to the decreased coupling between the dissipation layers in the loops. For linear resonant absorption the dissipation layer width decreases as $S^{-1/3}$ in a single loop (see, Ofman, et al., 1994).

Figure 7 shows the results of the 3D MHD model of an active region initiated with photospheric magnetic field extrapolated (potential) into the corona, and gravitationally stratified density. In normalized units the size of the Cartesian simulation box is $1 \times 0.53 \times 0.77$, and the lower boundary of the active region was at $z = 1$. The numerical resolution was $133 \times 71 \times 102$, and the Lundquist number was $S = 10^3$. A fast magnetosonic wave was launched at the $x - z$ plane towards the active region. Part of the wave energy is reflected by the active region and part is transmitted inducing damped oscillations in the active region's magnetic field (e.g., Ofman & Thompson, 2002). Figure 7c shows the temporal evolution of the velocity and the magnetic field components near the center of the active regions. About one full period of oscillations is evident at this location ($x = 0$, $y = 0$, $z = 1.2$ corresponding to $0.2R_\odot$ above the lower boundary of the active region). At higher altitudes, where the field strength is lower, additional oscillations are seen (this is evident in the animation of figure 7b). Note, that the fine structure of loop density as evident in TRACE observations and the above 3D MHD models of individual loops is not included in the model of the active region. Investigation of wave trapping effects of individual loops due to variations of the Alfvén speed inside the active region loops is planned in a future study.

4 Diagnostic from Wave Activity

The wave activity in loops and active regions can be used for the diagnostic of the magnetic field and other coronal properties as was demonstrated recently by Nakariakov & Ofman (2001). The accuracy of this tool depends strongly on the 3D information of the magnetic field structure, and on the accuracy of the 3D MHD models. Here, a list of possible diagnostics from wave activity is presented.

- From fast wave phase speed $V_f(x, y, z)$ one can determine $B(x, y, z)$, if $n(x, y, z)$, and $T(x, y, z)$ are known.
- Slow wave phase speed allows to determine the 3D temperature structure $T(x, y, z)$ of the active region loops.
- Individual loop oscillations provide information on localized density and Alfvén speed variations in the structure.
- Nonlinear waves allow to determine plasma β (this has been demonstrated by Terradas & Ofman, 2004a).

Note, that there are considerable difficulties in the interpretation and modelling of the observed oscillations due to mode coupling and nonlinearity, and the important role of fine structure which requires high resolution in numerical models and observations. The density and temperature can be obtained spectroscopically independently, in support of the wave diagnostic.

5 Conclusions

Wave activity is observed in active regions and individual loops in EUV by TRACE and SOHO EIT, and as Doppler shift oscillations by the SUMER instrument on SOHO following impulsive events. The observations of wave activity allows to determine important physical parameters of the coronal loops, such as the density, temperature, wave velocity, and the magnetic field. However, due to lack of three-dimensional information on the loops and active regions structure the analysis relies on modelling derived from images in the plane of the sky. Line of sight integration of optically thin emission and unknown filling factors further complicates the analysis. With the launch of the STEREO spacecraft two views of active regions will become available, and the 3D reconstruction will provide more accurate information on the active region loop structure. The observations could be used to initiate 3D MHD models of active region loops and wave activity in order to study the dynamics and stability and provide a new diagnostic tool of active region properties.

Several representative results of three dimensional MHD models of waves in loops and active regions with solar boundary conditions are shown here. The models are being constructed with the goal of developing wave diagnostic tools. Global oscillations were initiated in an active region by launching a fast wave towards the active region. The dynamics, and damping of the global oscillations were followed in the model. The initiation and damping of waves in individual loops, as well as a collection of four loops (that represents a multithreaded loop) was modelled with the isothermal, resistive 3D MHD code. By reproducing oscillations similar to observations by TRACE and EIT the models demonstrate that wave diagnostic is a feasible tool for the determination of active region and individual loop parameter. Stability of active region can be investigated with 3D MHD code as a bonus by following the evolution of the active region magnetized plasma on much longer (than oscillation period) time scale. Improved observations (e.g., three component magnetic field and flows, 3D density structure) used as initial and boundary conditions for the numerical models, combined with improved 3D MHD models (e.g, higher resolution, more realistic energy equation) will increase the reliability of this method.

Acknowledgments The author would like to thank NASA grants NNG04GA96G,

NAG5-11815, and NASA Sun-Earth Connection theory program.

References

Aschwanden, M. J., Fletcher, L., Schrijver, C. J., & Alexander, D. 1999, Astrophys. J., 520, 880

Aschwanden, M. J., De Pontieu, B., Schrijver, C. J., & Title, A. M. 2002, Solar Phys., 206, 99

Biesecker, D. A., Myers, D. C., Thompson, B. J., Hammer, D. M., & Vourlidas, A. 2002, Astrophys J., 569, 1009

De Moortel, I., Ireland, J., & Walsh, R. W. 2000, Astron. Astrophys., 355, L23

De Moortel, I., Ireland, J., Walsh, R. W., & Hood, A. W. 2002, Solar Phys., 209, 61

Goossens, M., Andries, J., & Aschwanden, M. J. 2002, Astron. Astrophys., 394, L39

Kliem, B., Dammasch, I. E., Curdt, W., & Wilhelm, K. 2002, Astrophys J., 568, L61.

Mendoza-Briceño, C. A., Erdélyi, R., & Sigalotti, L. D. 2004, Astrophys. J., 605, 493

Nakariakov, V.M., Ofman, L., DeLuca, E., Roberts, B., Davila, J.M. 1999, Science, 285, 862

Nakariakov, V.M., & Ofman, L. 2001, Astron. Astrophys., 372, L53

Ofman, L., Davila, J.M., Steinolfson, R.S. 1994, 421, 360

Ofman, L., & Davila, J.M. 1995, J. Geophys. Res., 100, 23427

Ofman, L. & Aschwanden, M. J. 2002, Astrophys. J., 576, L153

Ofman, L. & Wang, T. 2002, Astrophys. J., 580, L85

Ofman, L. & Thompson, B. J. 2002, Astrophys. J., 574, 440

Roberts, B. 2000, Solar Phys., 193, 139

Ruderman, M. S. & Roberts, B. 2002, Astrophys. J., 577, 475

Ruderman, M. S. 2003, Astron. Astrophys., 409, 287

Schrijver, C. J., Aschwanden, M. J., & Title, A. M. 2002, Solar Phys., 206, 69

Terradas, J. & Ofman, L. 2004, Astrophys. J., 610, 523

Terradas, J., Ofman, L. 2004, SOHO 13 'Waves, Oscillations and Small-Scale Transients Events in the Solar Atmosphere: A Joint View from SOHO and TRACE', 29 September - 3 October 2003 Palma de Mallorca, Balearic Islands, Spain, H. Lacoste, ESA SP-547. Noordwijk, the Netherlands: European Space Agency, p.469

Thompson, B. J., et al. 1999, Astrophys. J., 517, L151

Verwichte, E., Nakariakov, V.M., Ofman, L., DeLuca, E.E., 2004, Solar Phys., in press.

Wang, T.J., Solanki, S.K., Curdt, W., Innes, D.E., & Dammasch, I.E. 2002, Proc. 10th SOHO Workshop, Davos, Switzerland, March 2002.

Wang, T. J., Solanki, S. K., Innes, D. E., Curdt, W., & Marsch, E. 2003, Astron. Astrophys., 402, L17
Wills-Davey, M. J. & Thompson, B. J. 1999, Solar Phys., 190, 467
Wu, S. T., Zheng, H., Wang, S., Thompson, B. J., Plunkett, S. P., Zhao, X. P., & Dryer, M. 2001, J. Geophys. Res., 106, 25089

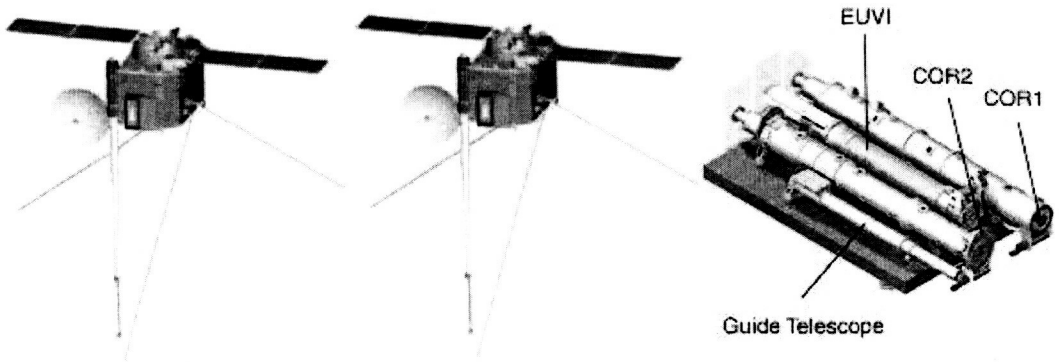

Fig. 1. The STEREO spacecraft (two left panels), and the EUV and coronagraph instruments (right panel) that will be carried by each spacecraft.

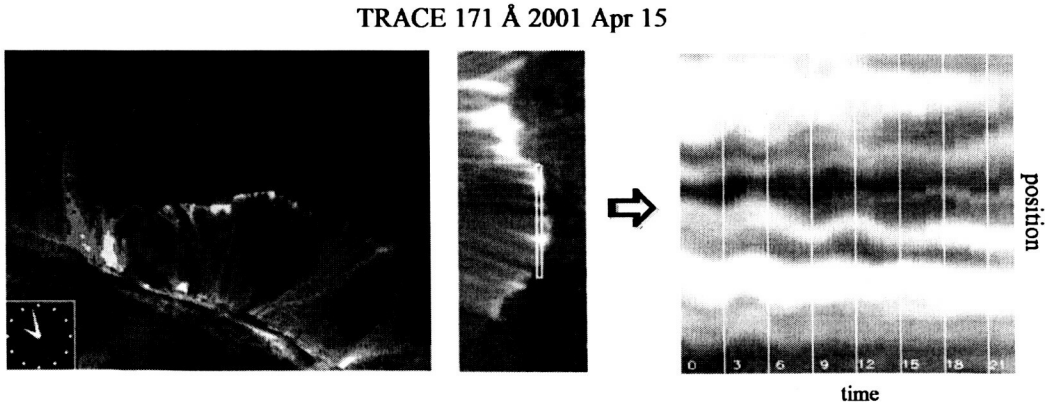

Fig. 2. Loop oscillations observed in an arcade by TRACE 171Å on April 15, 2001 (see, Aschwanden, et al, 2002; Verwichte et al., 2004).

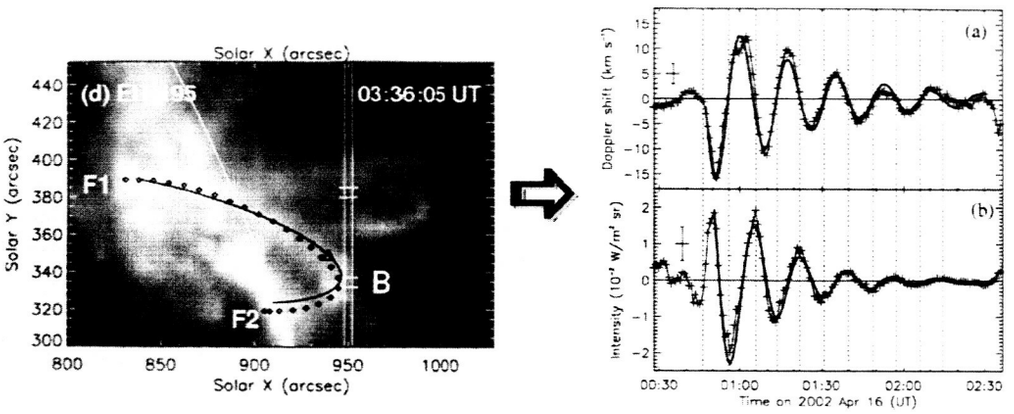

Fig. 3. Loop oscillations observed as (a) Doppler shift oscillations and (b) intensity oscillations by SOHO/SUMER. The left panel shows the outline of the loop as seen by EIT at 195 Å on April 15, 2002 (adapted from Wang et al., 2003).

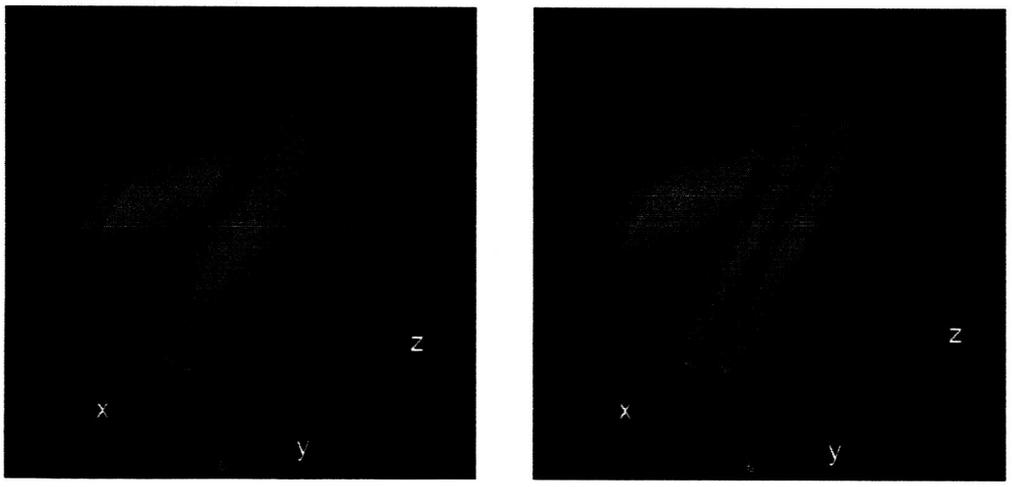

Fig. 4. 3D MHD model of active region loops impacted by an EIT wave. The left panel shows an isosurface of a single loop density with the magnetic field in the z direction. The right panel shows density isosurface of four closely spaced loops impacted by the wave. The intensity scale indicates the magnitude of the current density square (J^2) of the impacting wave in arbitrary units.

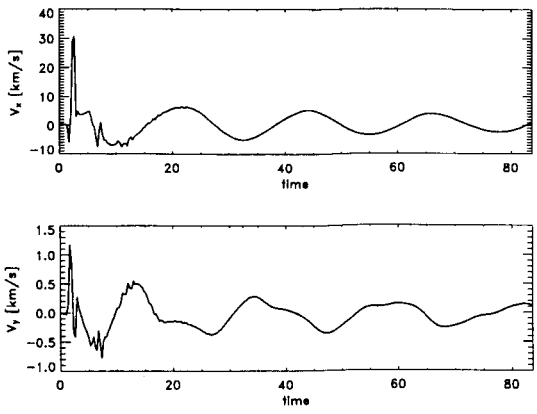

Fig. 5. The temporal evolution of the velocity of the single loop with the Lundquist number $S = 10^3$ at the point $x = 1.07$, $y = 2.70$, $z = 8.04$ in normalized units (located near the midpoint of loop length, and near the loop boundary). The top panel shows the damping of V_x (transverse oscillations). The V_y component corresponds to the internal Alfvén wave generated by the transverse oscillations.

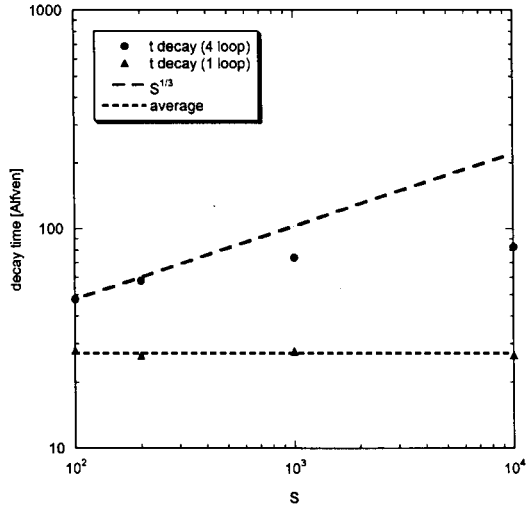

Fig. 6. The scaling of the damping time of loop oscillations with the Lundquist number S for a single loop, and for four loops. It is evident that the damping time is independent of resistivity for a single loop. However, for four loops the damping time increases with the Lundquist number. The scaling of phase mixing with S is shown with long dashes. The short dashes line indicates the average damping time for a single loop.

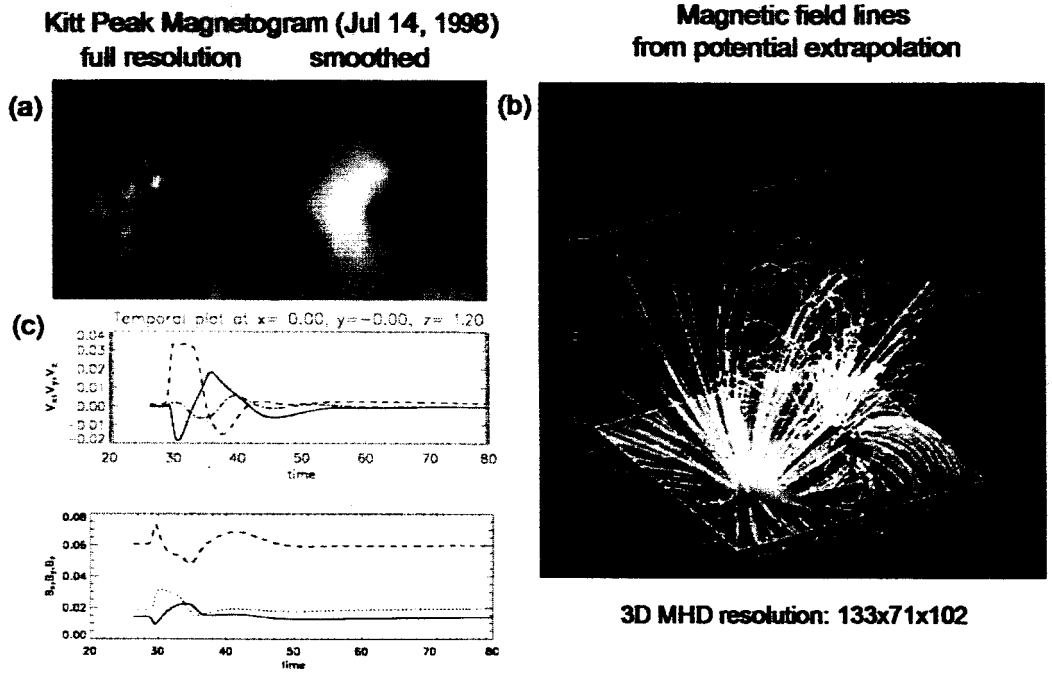

Fig. 7. Three dimensional MHD model of active region oscillations. (a) Kitt Peak magnetogram of the active region field taken on July 14, 1998 (left panel) is smoothed to the lower resolution of the 3D MHD model (right panel). (b) The 3D magnetic field structure is filled with gravitationally stratified plasma at $T = 2 \times 10^6$ K; the oscillations are excited by impacting fast wave at the active region boundary ($x - z$ plane). (c) Temporal evolution of the velocity and the magnetic field in the center of the active region.